Submitted 18-3-08. Revised 11-6-08. Accepted 15-7-08.

HYPEROSMOTIC STRESS INDUCES AXL ACTIVATION AND CLEAVAGE IN CEREBRAL ENDOTHELIAL CELLS

Imola Wilhelm[1], Péter Nagyőszi[1], Attila E. Farkas[1], Pierre-Olivier Couraud[2], Ignacio A. Romero[3], Babette Weksler[2], Csilla Fazakas[1], Ngo Thi Khue Dung[1], Sándor Bottka[4], Hannelore Bauer[5], Hans-Christian Bauer[5], and István A. Krizbai[1*]

[1]Institute of Biophysics, Biological Research Center, Szeged, Hungary,

[2]INSERM U567, Institut Cochin, Paris, France,

[3]The Open University, Milton Keynes, UK,

[4]Institute of Plant Biology, Biological Research Center, Szeged, Hungary,

[5]ABT, Dept. Org. Biology, University of Salzburg, Salzburg, Austria

[*]**Corresponding author:**

István A. Krizbai

Institute of Biophysics, Biological Research Center,

Temesvári krt. 62,

6726 Szeged, Hungary

Tel: 36-62-599602

Fax: 36-62-433133

E-mail: krizbai@brc.hu

Abbreviations:

BBB, blood-brain barrier

CECs, cerebral endothelial cells

DMNQ, 2,3-dimethyl-1,4-naphthoquinone

ERK, extracellular signal-regulated kinase

FAK, focal adhesion kinase

GAPDH, glutaraldehyde-3-phosphate dehydrogenase

Gas 6, growth arrest-specific protein 6

Ma, mannitol

PDTC, pyrrolidine dithiocarbamate

PI3K, phosphatidyl inositol 3-kinase

PMA, phorbol myristyl acetate

PKC, protein kinase C

ABSTRACT

Due to the relative impermeability of the blood-brain barrier many drugs are unable to reach the CNS in therapeutically relevant concentration. One method to deliver drugs to the CNS is the osmotic opening of the blood-brain barrier using mannitol. Hyperosmotic mannitol induces a strong phosphorylation on tyrosine residues in a broad spectrum of proteins in cerebral endothelial cells, the principal components of the blood-brain barrier. Previously we have shown that among targets of tyrosine phosphorylation are β-catenin, extracellular signal-regulated kinase 1/2 and the non-receptor tyrosine kinase Src. The aim of this study was to identify new signaling pathways activated by hypertonicity in cerebral endothelial cells. Using an antibody array and immunoprecipitation we identified the receptor tyrosine kinase Axl to become tyrosine phosphorylated in response to hyperosmotic mannitol. Besides activation, Axl was also cleaved in response to osmotic stress. Degradation of Axl proved to be metalloproteinase- and proteasome-dependent and resulted in 50-55 kDa C-terminal products which remained phosphorylated even after degradation. Specific knockdown of Axl increased the rate of apoptosis in hyperosmotic mannitol-treated cells, therefore we assume that activation of Axl may be a protective mechanism against hypertonicity-induced apoptosis. Our results identify Axl as an important element of osmotic stress-induced signaling.

Keywords: blood-brain barrier, cerebral endothelial cells, mannitol, hyperosmosis, Axl

Running title: Hyperosmotic phosphorylation and cleavage of Axl

INTRODUCTION

Cerebral endothelial cells (CECs) are the principal components of the blood-brain barrier (BBB). They form a continuous monolayer and are interconnected by tight junctions which impair the free movement of different chemical compounds from one side to the other side of the barrier. The cerebral microvasculature is ensheated by astrocytic endfeet which play an essential role in maintaining BBB phenotype (for review see: Abbott *et al* 2006). Low permeability of the endothelial cell monolayer protects the CNS from potentially toxic substances and contributes significantly to the homeostasis of the brain. Regulation of permeability is under complex control. In these regulatory processes signaling molecules, like protein kinases and phosphatases, cyclic nucleotides, calcium, etc. play important roles (Deli *et al* 1993; Hurst *et al* 1998; Lohmann *et al* 2004; Krizbai and Deli 2003).

From clinical point of view, due to the relative impermeability of the barrier many drugs are unable to reach the CNS in therapeutically relevant concentration, making the BBB one of the major impediments in the treatment of CNS disorders. A large number of strategies have been developed in order to circumvent this problem. One of the successfully used methods to deliver drugs — especially antitumoral agents — to the CNS is the osmotic opening of the BBB using mannitol (Kroll *et al* 1998; Neuwelt *et al* 1980; Neuwelt *et al* 1991). This causes a rapid opening (within minutes) of the BBB which is reversible. The barrier function starts to recover approximately 1 h after treatment, but complete recovery is achieved only after 6-8 h (Rapoport *et al* 1980; Siegal *et al* 2000).

Despite successful clinical trials the molecular mechanisms underlying the effect of hyperosmotic mannitol are largely unknown. Early studies were not able to detect any changes in the structure of the interendothelial tight junctions of brain capillary endothelial cells (Farrell *et*

al 1984), however, later Lossinsky *et al* (1995) have demonstrated that a single intracarotid injection of hypertonic 1.8 M L (+) arabinose widened interendothelial spaces. Peroxidase tracer was observed within vesiculo-tubular profiles, and occasionally within widened interendothelial junctional clefts. Furthermore, intraperitoneal infusion of hyperosmotic mannitol induced increased expression of AQP4 in astrocytes, at sites where the blood-brain barrier was disrupted (Arima *et al* 2003).

Hyperosmotic stress initiates a variety of compensatory and adaptive responses (for review see: Maurice *et al* 2007). In response to hypertonicity cells can initiate a rapid reorganization of the actin cytoskeleton. Di Ciano et al. have shown that hypertonic conditions induce submembranous de novo F-actin assembly and promote association of cortactin with the actin-related protein 2/3 (Arp2/3) complex (Di Ciano *et al* 2002). Further research has revealed activation of Rho, Rac and Cdc42 as well (Di Ciano-Oliveira *et al* 2003; Lewis *et al* 2002). Our atomic force microscopic studies have revealed a significant decrease in cell height and elasticity accompanied by the appearance of cytoplasmic protrusions (Balint *et al* 2007).

There is increasing evidence that hypertonicity induces a concerted action of signaling mechanisms. Protein phosphorylation plays an important role in the cellular adaptation to hyperosmotic conditions and cellular shrinkage. It has been shown that one target of phosphorylation is cortactin, an actin-binding protein which is phosphorylated in a Fyn-dependent manner in Chinese hamster ovary cells (Kapus *et al* 1999). Another target protein of hyperosmotic stress-stimulated phosphorylation is focal adhesion kinase (FAK) which becomes phosphorylated on Tyr-397 and Tyr-577 via a Src-independent pathway in fibroblats and epithelial cells (Lunn *et al* 2004). However, less is known about endothelial, especially cerebral endothelial cells. In our previous study we have shown that β-catenin becomes tyrosine

phosphorylated in response to mannitol in CECs and this phosphorylation is Src kinase-dependent (Farkas *et al* 2005).

The aim of this study was to identify new signaling pathways regulated by hyperosmosis in CECs.

MATERIAL AND METHODS

Materials

All chemicals, if not otherwise stated, were purchased from Sigma.

The following inhibitors were used: genistein, PP1, Y27632 (Tocris), GM6001, calpeptin, bisindolylmaleinimide, MG132, zVAD (Calbiochem), DMNQ, pyrrolidine dithiocarbamate (PDTC), sodium vanadate, verapamil (Sigma), leupeptin, E64, pepstatin, pefabloc (Roche), U0126 (Cell Signaling), wortmannin (Alomone).

Protein G Sepharose was purchased from GE Healthcare. We have used the following antibodies: anti-Axl (C20) (Santa Cruz), anti-Akt, anti-phospho-Akt (Ser473), anti-cleaved caspase-3 (Asp175) (Cell Signaling), anti-phosphotyrosine, anti-β-actin (Sigma), HRP-anti-goat IgG (Santa Cruz), HRP-anti-mouse IgG (Sigma), HRP-anti-rabbit IgG (Cell Signaling), Cy3-anti-goat IgG and -anti-rabbit IgG (Jackson).

Cell culture and treatments

The human cerebral endothelial cell line hCMEC/D3 was maintained as described previously (Weksler *et al* 2005). Briefly, the cells were grown on rat tail collagen coated plates or glass coverslips in EBM-2 medium (Cambrex) supplemented with EGM-2 Bullet Kit (Cambrex) and 2.5% fetal bovine serum (FBS, Sigma).

Confluent monolayers of hCMEC/D3 cells were treated in serum free culture medium with 10-20% mannitol (0.55-1.1 M, corresponding to an additional 550-1100 mOsmol/l compared to the 300 mOsmol/l control) and various other substances were added concurrently with mannitol as indicated. Genistein treatment was performed with an 1 h preincubation.

Antibody array

For the detection of phosphorylated proteins we used an antibody array (Hypromatrix) and followed the manufacturer's recommendations during the whole procedure. Briefly, cells were lysed in a buffer containing 20 mM Tris, 150 mM NaCl, 1 mM EDTA, 1% Triton X-100, 1 mM sodium vanadate, 10 mM NaF, 1 mM Pefabloc. After centrifugation (10,000 x g, 10 min, 4°C) the cell homogenate was incubated with the antibody matrix. Following washing steps, the membrane was incubated with HRP-labeled anti-phosphotyrosine antibody (Hypromatrix) and the reaction was visualized using ECL Plus (GE Healthcare).

Western-blot

Cells were washed with phosphate buffered saline (PBS) and scraped into ice-cold lysis buffer (20 mM Tris, 150 mM NaCl, 1 mM EDTA, 1% Triton X-100, 1% sodium deoxycholate, 0.1% sodium dodecyl sulphate, 1 mM sodium vanadate, 10 mM NaF, 1 mM Pefabloc) and incubated on ice for 30 min. For determination of water- and detergent soluble proteins the following buffers were used: 20 mM Tris, 150 mM NaCl, 1 mM EDTA, 1 mM sodium vanadate, 10 mM NaF, 1 mM Pefabloc for water-soluble proteins, and the same buffer containing in addition 1% TritonX-100 for detergent-soluble proteins. Lysates were clarified by centrifugation at 10,000 x g for 10 min on 4°C and protein concentration was determined with the BCA method (Pierce). Proteins were electrophoresed and blotted onto PVDF (Pall) or nitrocellulose

(Schleicher-Schuell) membranes. The immunoreaction was visualized using ECL Plus chemiluminescence detection kit.

Immunoprecipitation

For immunoprecipitation experiments cells were homogenized in lysis buffer as described above. Briefly, lysates were centrifuged at 10,000 x g for 10 min in a microfuge and the supernatant was subjected to immunoprecipitation. After preclearing with protein G Sepharose, supernatants were incubated with 2-5 µg primary antibody (anti-phosphotyrosine or -Axl) at 4°C for 4 h. The formed immunocomplexes were precipitated by incubating the samples overnight with protein G Sepharose beads. The precipitates were washed 4 times with lysis buffer, boiled in sample buffer, and subjected to electrophoresis and immunoblotting.

Specific knockdown of Axl by RNA interference

Stealth™ siRNA duplex oligoribonucleotides were designed using Invitrogen BLOCK-iT™ RNAi designer and were purchased from Invitrogen. The sequences used were as follows: sense, 5'-CAGGAACTGCATGCTGAATGAGAA-3'; antisense, 5'-TTCTCATTCAGCATGCAGTTCCTGG-3'. As control non-targeting RNA we have used the following scrambled oligonucleotides: sense, 5'-GACGTAGAGAGAGTTCCGACATACA-3' and antisense 5'-TGTATGTCGGAACTCTCTCTACGTC-3'. Briefly, cells were plated at 50% confluency. Transfection of oligonucleotides was then performed in OptiMEM medium containing 10 nM RNA and Lipofectamine™ RNAiMAX reagent (Invitrogen) following the manufacturer's instructions. After 6 h the medium was changed to regular culture medium. In order to increase the efficiency, a second transfection was performed the following day. Cells were analyzed 24 h after the second transfection when they achieved confluency.

Immunofluorescence

Cells were fixed using a mixture of ice cold ethanol : acetic acid (95:5) for 10 min. After blocking with 3% bovine serum albumin for 30 min, coverslips were incubated with primary antibody. The staining was visualized using Cy3-conjugated secondary antibody. Coverslips were mounted in anti-fading embedding medium (Biomeda) and the distribution of the signal was studied using a Nikon Eclipse TE2000U photomicroscope with epifluorescent capabilities connected to a digital camera (Spot RT KE).

Real-time PCR

For real-time PCR analysis we isolated total RNA from treated and untreated cells using TRIzol reagent (Invitrogen) following the manufacturer's recommendations. RNA was transcribed into cDNA using a reverse transcription kit (Fermentas). The amplification was performed on a BioRad iQ5 instrument using FastStart SYBR Green Mix (Roche) under the following conditions: 30 cycles of 95°C for 15 s, 55°C for 30 s, 72°C for 30 s.

The following primer pairs were used for amplification: GAS6: 5'-TGCTGTCATGAAAATCGCGG-3' and 5'-CATGTAGTCCAGGCTGTAGA-3', Axl: 5'-GGTGGCTGTGAAGACGATGA-3' and 5'-CTCAGATACTCCATGCCACT-3' (Sun *et al* 2002), GAPDH (glutaraldehyde-3-phosphate dehydrogenase) (control): 5'-GTGAAGGTCGGTGTCAACG-3' and 5'-GTGAAGACGCCAGTAGACTC-3'. Determination of threshold cycle and quantitation was performed using the software of the instrument.

Two-dimensional electrophoresis coupled with Western-blot

Control and mannitol treated cells were washed with Tris buffered sorbitol (10 mM Tris, 25 mM sorbitol, pH=7.0) and scraped into sample-rehydration buffer (7 M urea, 2 M thiourea, 2% CHAPS, 1% DTT, 0.2 mM vanadate, 1 mM Pefabloc, 1 mM NaF, 0.2% ampholite, traces of bromophenol blue) and incubated at room temperature for 1 h. Debris was removed by centrifugation at 16,000 x g for 20 min on 17°C. The two-dimensional electrophoresis was carried out on a Protean IEF Cell using immobilized pH gradient strips (7 cm, pH 4-7 BioRad Laboratories Inc.) and a Mini-Protean 3 cell according to the manufacturer's instructions. Western-blots were performed on the second dimension gels.

Determination of apoptosis

Cells cultured on glass coverslips were transfected with Axl siRNA construct (as described previously), followed by treatment with 20% mannitol for 3 h. In order to control the efficiency of silencing, parallel Western-blot analysis was performed using anti-Axl antibody (as described previously). Immunofluorescence staining was done using anti-cleaved caspase-3 antibody (according to the manufacturer's instructions). 1,000 cells/coverslip were analyzed under fluorescence microscope and labelled cells were counted. In another set of experiments nuclear morphology was analysed using Hoechst 33342 staining (0.6 µg/ml). Nuclei containing condensed chromatin at the nuclear envelope or fragmented chromatin were considered apoptotic (Bresgen *et al* 2003).

RESULTS

Phosphorylation of Axl

In our previous studies we have shown that hyperosmotic mannitol induces a strong phosphorylation on tyrosine residues in CECs (Farkas *et al* 2005). To further identify target proteins of tyrosine phosphorylation an antibody array screening was applied using a matrix loaded with antibodies directed mainly against signaling molecules. Using this method we found β-catenin, the MAPkinase extracellular signal-regulated kinase (ERK)1, p130Cas, focal adhesion kinase (FAK) and the receptor tyrosine kinase Axl to become phosphorylated (Fig. 1A). In our previous studies we have already shown that β-catenin and ERK are targets of mannitol induced phosphorylation in CECs. Literature data are available confirming the phosphorylation of p130Cas and FAK in response to hyperosmosis (Ueno *et al* 2001; Lunn *et al* 2004).

To prove that Axl can indeed be phosphorylated under hypertonic conditions we performed immunoprecipitation studies using anti-phosphotyrosine antibody (Fig. 1B) and anti-Axl antibody as well (Fig. 1C). Both approaches confirmed the tyrosine phosphorylation of Axl after treatment of the cells with 20% mannitol for 30 min.

Activation of Akt

To test the activation of the possible downstream elements of Axl signaling we investigated the phosphorylation of Akt (protein kinase B). RNA interference was used to specifically knock down Axl and the result of silencing was controlled using Western-blot with anti-Axl antibody (Fig. 2A). An almost complete silencing of Axl protein could be achieved. We found that mannitol was able to induce the phosphorylation (on Ser473 residue) and thus the activation of

Akt (Fig. 2B). This phenomenon was prevented by Axl silencing, showing that mannitol induced Akt activation occurs through the receptor tyrosine kinase Axl.

Degradation of Axl

We have observed that besides phosphorylation, treatment of CECs with 20% mannitol induced the appearance of a double proteolytic band with an apparent molecular weight of 50-55 kDa (arrowheads, Fig. 1B, 3A) accompanied by a decrease in the intensity of the full size Axl band (Fig. 1B, 3A). Since our antibody recognizes the C-terminal of the protein, we conclude that this degradation band corresponds to the intracellular domain of Axl. Degradation of Axl proved to be time- and concentration-dependent and was clearly detectable after 10 min of mannitol treatment (Fig. 3B).

Changes in the localization of Axl in response to mannitol treatment

Results obtained with Western-blot analysis were supported by immunofluorescence studies as well. Under control conditions Axl staining was diffuse, whereas treatment of CECs with 20% mannitol led to the appearance of a conspicuous perinuclear staining (Fig. 4).

Regulation of Axl and Gas6 at mRNA level

To test if mannitol is able to regulate Axl at transcriptional level, we performed real-time PCR experiments. We could not observe changes in the expression of either Axl or its ligand Gas6 in response to mannitol treatment (Fig. 5).

Effect of different stress factors on Axl degradation

We have tested the effect of other osmotic agents (arabinose, sodium chloride and urea) in similar osmotic concentrations to 1.1 M mannitol (additional 1100 mOsmol/l). When osmotic stress was caused by poorly cell permeable agents (mannitol, NaCl or arabinose) we observed the appearance of the cleavage products with a parallel decrease in the main Axl band (Fig. 6A). However, the cell permeable urea did not induce Axl cleavage (Fig. 6A), suggesting that cellular shrinkage is probably responsible for Axl degradation. Other stress factors like oxidative stress (DMNQ treatment), calcium or glucose deprivation (not shown) or high glucose concentration (8 g/l) did not cause alterations in Axl levels (Fig. 6B). Degradation of Axl in response to hypertonic stress could be detected not only in CECs but in other cell types like Madine Darby Canine Kidney (MDCK) or the rat glioma cell line RG2 as well (Fig. 6C).

Mechanism of Axl cleavage

To identify the mechanisms by which Axl degradation is regulated we have used a series of inhibitors of different signaling pathways and protease inhibitors. Inhibition of nuclear factor-kappa B (NFκB, using PDTC), Rho-kinase (using Y27632), calcium channel (using verapamil), protein kinase C (PKC, using bisindolylmaleimide), phosphatidyl inositol 3-kinase (PI3K, using wortmannin), ERK 1/2 (using U0126) or Src kinase (using PP1) did not affect the degradation of Axl. Caspase inhibition (using zVAD), inhibition of calpain (using calpeptin), and the use of cysteine, serine or aspartic protease inhibitors (E64, leupeptin, pepstatin) were also ineffective in reducing the degradation of Axl (Fig. 7A, B and C). On the other hand, the matrix metalloproteinase inhibitor GM6001 was able to almost completely inhibit the degradation of Axl induced by mannitol (Fig. 8A and B).

We investigated the solubility of the different Axl bands. Only the lower band of the degradation products proved to be soluble in detergent-free buffer. Both the whole protein and the upper degradation band were water-insoluble and detergent (i.e. TritonX-100) soluble (Fig. 8C). The proteasome inhibitor MG132 induced the disappearance of the lower (water-soluble) degradation fragment parallelly with the intensification of the upper (detergent-soluble) cleavage product, however, no change in the amount of the 140 kDa band was seen (Fig. 7B and 8C).

Phosphorylation and degradation of Axl

To study the possible relationship between the phosphorylation and degradation of Axl we investigated the time course of Axl phosphorylation and degradation. Axl becomes phosphorylated after 2 min and reaches its maximum at 15 min whereas the degradation starts between 5-15 min (Fig. 9A). Pervanadate, a strong phosphatase inhibitor induced the phosphorylation of Axl but did not cause its degradation indicating that the cleavage of Axl is not induced by tyrosine phosphorylation (Fig. 9B). This was also supported by the fact that the tyrosine kinase inhibitor genistein, which inhibited the phosphorylation of Axl, did not inhibit its degradation (Fig. 9B). Furthermore, the metalloproteinase inhibitor GM6001 which inhibited the degradation of Axl did not affect activation of Akt, a downstream element of Axl signaling (Fig. 9C).

Our results obtained from phosphotyrosine immunoprecipitation studies suggest that the degradation products of Axl are phosphorylated in mannitol treated cells (double arrowheads on Fig. 9B and 1B and C). The tyrosine kinase inhibitor genistein reduced the mannitol-induced phosphorylation of the Axl degradation products to control levels (Fig. 9B). Presence of multiple spots at the level of the 55 kDa degradation products on Axl Western-blots performed on two-dimensional gels may also indicate differentially phosphorylated forms of the protein (Fig. 9D).

Role of Axl in mannitol-induced apoptosis

To gain insight into the role of mannitol-induced Axl activation we have counted the number of apoptotic cells after mannitol treatment in control and Axl-silenced cells. The knockdown was almost complete in Axl siRNA-transfected cells, however, the scrambled sequence did not affect Axl expression (Fig. 10A). The rate of apoptosis was determined based on cleaved caspase-3 staining. 30 min mannitol treatment did not induce significant changes in the number of apoptotic cells. However, after 3 h mannitol treatment a more than 100% increase was detectable: from 2.83±0.10% in Lipofectamine treated and 2.55±0.21% in scrambled RNA-transfected cells to 5.83±0.21% and 5.50±0.85%, respectively (Fig. 10B). Axl silencing induced a more than 50% increase in the number of apoptotic cells in control conditions, and a more than 40% increase in mannitol treated cells (Fig. 10B). Similar results were obtained when apoptosis was assessed based on nuclear morphology (not shown).

DISCUSSION

Experiments of the present study were designed to identify signaling mechanisms activated by hyperosmotic stress in CECs. In our previous studies (Farkas *et al* 2005) we have shown that mannitol induces a strong phosphorylation on tyrosine residues in a broad spectrum of proteins ranging between 50-200 kDa. We have further shown that among targets of tyrosine phosphorylation are β-catenin and the non-receptor tyrosine kinase Src. Here by using a screening approach based on an antibody array we could identify three additional proteins to become tyrosine phosphorylated in response to hyperosmotic stress: p130Cas (p130 Crk-associated substrate), FAK (focal adhesion kinase) and Axl. Moreover, we could confirm our

earlier finding that β-catenin and ERK1 are tyrosine phosphorylated in CECs in response to hyperosmotic mannitol treatment.

p130Cas is an Src substrate signaling molecule localized to focal adhesions (Harte *et al* 1996) and is involved in several processes including motility, adhesion, proliferation and survival (for review see: Defilippi *et al* 2006). p130Cas has already been shown to become tyrosine phosphorylated in adipocytes in response to osmotic stress (Ueno *et al* 2001). FAK which is in close interaction with p130Cas (Polte *et al* 1995) has also been shown to be tyrosine phosphorylated under hyperosmotic conditions in fibroblasts and endothelial cells of non-cerebral origin (Lunn *et al* 2004; Malek *et al* 1998).

Axl (also called ARK, UFO and Tyro7) is a member of a family of receptor tyrosine kinases that includes Mer and Sky, having the vitamin K-dependent Gas 6 (growth arrest-specific protein 6) as its natural ligand (for review see: Hafizi and Dahlback 2006a, 2006b). This family of receptor tyrosine kinases is characterized by two immunoglobulin-like and two fibronectin type III domains in the N-terminal region and a tyrosine kinase domain in the intracellular C-terminal region. Axl has two alternatively spliced forms (O'Bryan *et al* 1995) that either contain or lack 9 amino acids carboxyl-terminal to the fibronectin domains in the extracellular part of the protein. Axl is emerging as a regulator of a large number of cellular functions and has been shown to be involved in the regulation of different aspects of endothelial function as well. It has been demonstrated that activation of Axl can rescue endothelial cells from apoptosis (D'Arcangelo *et al* 2006; D'Arcangelo *et al* 2002; Hasanbasic *et al* 2004) and Axl is involved in cell migration and vascular remodeling (Korshunov *et al* 2007; Korshunov *et al* 2006) and angiogenesis (Gallicchio *et al* 2005; Holland *et al* 2005) as well.

Activation of Axl results in autocatalytic tyrosine phosphorylation, recruitment of different signaling molecules (Grb2 and the p85 subunit of phosphatidylinositol-3 kinase) (Weinger *et al*

2008) and activation of downstream elements like Akt. By demonstrating that Akt is phosphorylated on Ser473 residue only in cells expressing Axl we could identify a new signaling pathway activated by osmotic stress in CECs.

Furthermore we have shown that Axl is cleaved in response to hyperosmosis, the C-terminal products having an apparent molecular weight of about 50-55 kDa. Axl has been shown to be posttranslationally regulated by proteolysis (O'Bryan *et al* 1995) resulting in the generation of soluble Axl (Costa *et al* 1996). Our results show that the mannitol-induced cleavage of Axl is metalloproteinase-dependent which is in line with previous reports demonstrating the role of disintegrin-like metalloproteinase ADAM 10 in the cleavage of Axl (Budagian *et al* 2005). The role of Axl cleavage and the function of soluble Axl is still far from being completely understood. Soluble Axl has been detected in mouse serum and is constitutively released by murine primary and transformed cells (Budagian *et al* 2005). It may play role in the regulation of the bioavailabilty of the Axl ligand Gas6 by binding and thus inactivating it. Activation of PKC has also been shown to trigger cleavage of Axl and the proteolytic cleavage site was found to localize to a 14-amino acid region (VKEPSTPAFSWPWW) between the second fibronectin and the transmembrane domain (O'Bryan *et al* 1995). However, in CECs the PKC inhibitor bisindolylmaleimide was able to inhibit only PMA (phorbol myristyl acetate)-, but not hyperosmosis-induced Axl degradation (data not shown) suggesting that there is a difference between hyperosmosis- and PKC-induced Axl degradation.

It is well known that Axl is expressed at high levels in gliomas, mediating both tumor growth and angiogenesis (Vajkoczy *et al* 2006). Specific targeting of Axl may become a promising target of therapy of these tumors. Our results have shown that hyperosmotic mannitol-induced cleavage of Axl was not restricted to cerebral endothelial, or tight junction-expressing (endothelial and epithelial) cells, but glioma cells as well. Interestingly, when NaCl or arabinose

were used instead of mannitol in the same osmotic concentration Axl cleavage occured in the same way, however, the cell permeable urea did not induce Axl degradation. Therefore, we assume that cellular shrinkage might be responsible for this phenomenon.

We found that induction of tyrosine phosphorylation of Axl did not lead to its degradation, and inhibition of tyrosine phosphorylation did not influence the mannitol-induced cleavage of Axl. These findings suggest that there is no direct relationship between phosphorylation and cleavage of Axl. Using an antibody recognizing the C-terminal region of Axl we have observed that the degradation products containing the catalitically active intracellular domain of Axl remain phosphorylated. Mainly the upper (TritonX-100 soluble) degradation band proved to be phosphorylated, however, the two degradation bands seem to be different cleavage products and not differently phosphorylated forms of the same cleavage products. This is supported by the fact that treatment with genistein which inhibited the phosphorylation of Axl, did not inhibit the appearance of two cleavage products (Fig. 9B). Moreover, the appearance of the lower degradation band was prevented by the proteasome inhibitor MG132 (Fig. 7B and 8C) supporting that in hyperosmotic mannitol-treated cells the metalloproteinase-mediated cleavage was followed by a proteasomal cleavage, resulting in a water-soluble degradation product.

In order to address the functional implications of Axl activation, we have performed knockdown experiments and examined hyperosmotic mannitol-induced apoptosis. It is well documented that hypertonicity induces apoptosis in different cell types (for review see: Bortner and Cidlowski 2007). On the other hand, activation of the Axl-Akt pathway is involved in cell survival and anti-apoptotic mechanisms (for review see: Hafizi and Dahlback 2006b). We have found an approximately 90-100% increase in apoptosis after treatment with hyperosmotic mannitol. The relatively low absolute levels of apoptosis are apparently in contrast with previous observations by Malek *et al* (1998), who have shown that treatment of bovine aortic endothelial

cells with 600 mOsmol/l mannitol for 3 h induced an increase in the rate of apoptosis from 1.2% to 42%. However, microvascular endothelial cells may react differently to apoptotic stimuli than macrovascular endothelial cells. It has been shown that hyperglycaemic conditions significantly increased apoptosis in macrovascular endothelial cells, while increasing viability and inhibiting apoptosis in microvascular endothelial cells (Duffy *et al* 2006). In our previous study we have shown that prolonged oxidative stress even under hypoglycaemic conditions was able to induce an apoptosis of about 7-20% with a great interspecies variability (Bresgen *et al* 2003). We observed that Axl silencing increased the rate of apoptosis in hyperosmotic mannitol-treated cells, therefore we assume that activation of Axl may be a protective mechanism against mannitol-induced apoptosis.

Further studies are needed to clarify if Axl is involved in the hyperosmotic mannitol-induced BBB opening. A direct relationship between Axl signaling and proteins of the tight junction has not been shown so far. However, it is well known that a large number of signaling pathways are able to regulate junctional functions and tyrosine phosphorylation may play an important role in this process.

Taken together, our results identify Axl as an important element of hyperosmosis-induced signaling in cerebral endothelial cells, and suggest that Axl could play an important role in the adaptive response of cells to hyperosmotic stress.

Acknowledgements

This work was supported by NKTH XTTP SRT1 and GVOP-2004-0052/3.

REFERENCES

Abbott N. J., Rönnbäck L., Hansson E. (2006) Astrocyte-endothelial interactions at the blood-brain barrier. *Nat. Rev. Neurosci.* **7**, 41-53.

Arima H., Yamamoto N., Sobue K., Umenishi F., Tada T., Katsuya H., Asai K. (2003) Hyperosmolar mannitol simulates expression of aquaporins 4 and 9 through a p38 mitogen-activated protein kinase-dependent pathway in rat astrocytes. *J. Biol. Chem.* **278**, 44525-34.

Balint Z., Krizbai I. A., Wilhelm I., Farkas A. E., Parducz A., Szegletes Z., Varo G. (2007) Changes induced by hyperosmotic mannitol in cerebral endothelial cells: an atomic force microscopic study. *Eur. Biophys. J.* **36**, 113-20.

Bortner C. D., Cidlowski J. A. (2007) Cell shrinkage and monovalent cation fluxes: role in apoptosis. *Arch. Biochem. Biophys.* **462**, 176-88.

Bresgen N., Karlhuber G., Krizbai I., Bauer H., Bauer H. C., Eckl P. M. (2003) Oxidative stress in cultured cerebral endothelial cells induces chromosomal aberrations, micronuclei, and apoptosis. *J. Neurosci. Res.* **72**, 327-33.

Budagian V., Bulanova E., Orinska Z. et al. (2005) Soluble Axl is generated by ADAM10-dependent cleavage and associates with Gas6 in mouse serum. *Mol. Cell. Biol.* **25**, 9324-39.

Burg M. B., Ferraris J. D., Dmitrieva N. I. (2007) Cellular response to hyperosmotic stresses. *Physiol. Rev.* **87**, 1441-74.

Costa M., Bellosta P., Basilico C. (1996) Cleavage and release of a soluble form of the receptor tyrosine kinase ARK in vitro and in vivo. *J. Cell. Physiol.* **168**, 737-44.

D'Arcangelo D., Ambrosino V., Giannuzzo M., Gaetano C., Capogrossi M. C. (2006) Axl receptor activation mediates laminar shear stress anti-apoptotic effects in human endothelial cells. *Cardiovasc. Res.* **71**, 754-63.

D'Arcangelo D., Gaetano C., Capogrossi M. C. (2002) Acidification prevents endothelial cell apoptosis by Axl activation. *Circ. Res.* **91**, e4-e12.

Defilippi P., Di Stefano P., Cabodi S. (2006) p130Cas: a versatile scaffold in signaling networks. *Trends. Cell. Biol.* **16**, 257-63.

Deli M. A., Joo F., Krizbai I., Lengyel I., Nunzi M. G., Wolff J. R. (1993) Calcium/calmodulin-stimulated protein kinase II is present in primary cultures of cerebral endothelial cells. *J. Neurochem.* **60**, 1960-3.

Di Ciano-Oliveira C., Sirokmany G., Szaszi K., Arthur W. T., Masszi A., Peterson M., Rotstein O. D., Kapus A. (2003) Hyperosmotic stress activates Rho: differential involvement in Rho kinase-dependent MLC phosphorylation and NKCC activation. *Am. J. Physiol. Cell. Physiol.* **285**, C555-66.

Di Ciano C., Nie Z., Szaszi K., Lewis A., Uruno T., Zhan X., Rotstein O. D., Mak A., Kapus A. (2002) Osmotic stress-induced remodeling of the cortical cytoskeleton. *Am. J. Physiol. Cell. Physiol.* **283**, C850-65.

Duffy A., Liew A., O'Sullivan J., Avalos G., Samali A., O'Brien T.D. (2006) Distinct effects of high-glucose conditions on endothelial cells of macrovascular and microvascular origins. *Endothelium* **13,** 9-16.

Farkas A., Szatmari E., Orbok A. et al. (2005) Hyperosmotic mannitol induces Src kinase-dependent phosphorylation of beta-catenin in cerebral endothelial cells. *J. Neurosci. Res.* **80**, 855-61.

Farrell C. L., Shivers R. R. (1984) Capillary junctions of the rat are not affected by osmotic opening of the blood-brain barrier. *Acta. Neuropathol. (Berl.)* **63**, 179-89.

Gallicchio M., Mitola S., Valdembri D., Fantozzi R., Varnum B., Avanzi G. C., Bussolino F. (2005) Inhibition of vascular endothelial growth factor receptor 2-mediated endothelial cell activation by Axl tyrosine kinase receptor. *Blood* **105**, 1970-6.

Hafizi S., Dahlback B. (2006a) Gas6 and protein S. Vitamin K-dependent ligands for the Axl receptor tyrosine kinase subfamily. *FEBS. J.* **273**, 5231-44.

Hafizi S., Dahlback B. (2006b) Signalling and functional diversity within the Axl subfamily of receptor tyrosine kinases. *Cytokine Growth Factor Rev.* **17**, 295-304.

Harte M. T., Hildebrand J. D., Burnham M. R., Bouton A. H., Parsons J. T. (1996) p130Cas, a substrate associated with v-Src and v-Crk, localizes to focal adhesions and binds to focal adhesion kinase. *J. Biol. Chem.* **271**, 13649-55.

Hasanbasic I., Cuerquis J., Varnum B., Blostein M. D. (2004) Intracellular signaling pathways involved in Gas6-Axl-mediated survival of endothelial cells. *Am. J. Physiol. Heart. Circ. Physiol.* **287**, H1207-13.

Holland S. J., Powell M. J., Franci C., et al (2005) Multiple roles for the receptor tyrosine kinase axl in tumor formation. *Cancer. Res.* **65**, 9294-303.

Hurst R. D., Clark J. B. (1998) Alterations in transendothelial electrical resistance by vasoactive agonists and cyclic AMP in a blood-brain barrier model system. *Neurochem. Res.* **23**, 149-54.

Kapus A., Szaszi K., Sun J., Rizoli S., Rotstein O. D. (1999) Cell shrinkage regulates Src kinases and induces tyrosine phosphorylation of cortactin, independent of the osmotic regulation of Na+/H+ exchangers. *J. Biol. Chem.* **274**, 8093-102.

Korshunov V. A., Daul M., Massett M. P., Berk B. C. (2007) Axl Mediates Vascular Remodeling Induced by Deoxycorticosterone Acetate Salt Hypertension. *Hypertension* **50,** 1057-62.

Korshunov V. A., Mohan A. M., Georger M. A., Berk B. C. (2006) Axl, a receptor tyrosine kinase, mediates flow-induced vascular remodeling. *Circ. Res.* **98**, 1446-52.

Kroll R. A., Neuwelt E. A. (1998) Outwitting the blood-brain barrier for therapeutic purposes: osmotic opening and other means. *Neurosurgery* **42**, 1083-99.

Krizbai I. A., Deli M. A. (2003) Signalling pathways regulating the tight junction permeability in the blood-brain barrier. *Cell. Mol. Biol. (Noisy-le-grand)* **49**, 23-31.

Lewis A., Di Ciano C., Rotstein O. D., Kapus A. (2002) Osmotic stress activates Rac and Cdc42 in neutrophils: role in hypertonicity-induced actin polymerization. *Am. J. Physiol. Cell. Physiol.* **282**, C271-9.

Lohmann C., Krischke M., Wegener J., Galla H. J. (2004) Tyrosine phosphatase inhibition induces loss of blood-brain barrier integrity by matrix metalloproteinase-dependent and -independent pathways. *Brain. Res.* **995**, 184-96.

Lossinsky A. S., Vorbrodt A. W., Wisniewski H. M. (1995) Scanning and transmission electron microscopic studies of microvascular pathology in the osmotically impaired blood-brain barrier. *J. Neurocytol.* **24,** 795-806.

Lunn J. A., Rozengurt E. (2004) Hyperosmotic stress induces rapid focal adhesion kinase phosphorylation at tyrosines 397 and 577. Role of Src family kinases and Rho family GTPases. *J. Biol. Chem.* **279**, 45266-78.

Malek A. M., Goss G. G., Jiang L., Izumo S., Alper S. L. (1998) Mannitol at clinical concentrations activates multiple signaling pathways and induces apoptosis in endothelial cells. *Stroke* **29**, 2631-40.

Neuwelt E. A., Frenkel E. P., Diehl J., Vu L. H., Rapoport S., Hill S. (1980) Reversible osmotic blood-brain barrier disruption in humans: implications for the chemotherapy of malignant brain tumors. *Neurosurgery* **7**, 44-52.

Neuwelt E. A., Goldman D. L., Dahlborg S. A., Crossen J., Ramsey F., Roman-Goldstein S., Braziel R., Dana B. (1991) Primary CNS lymphoma treated with osmotic blood-brain barrier disruption: prolonged survival and preservation of cognitive function. *J. Clin. Oncol.* **9**, 1580-90.

O'Bryan J. P., Fridell Y. W., Koski R., Varnum B., Liu E. T. (1995) The transforming receptor tyrosine kinase, Axl, is post-translationally regulated by proteolytic cleavage. *J. Biol. Chem.* **270**, 551-7.

Polte T. R., Hanks S. K. (1995) Interaction between focal adhesion kinase and Crk-associated tyrosine kinase substrate p130Cas. *Proc. Natl Acad. Sci. USA* **92**, 10678-82.

Rapoport S. I., Fredericks W. R., Ohno K., Pettigrew K. D. (1980) Quantitative aspects of reversible osmotic opening of the blood-brain barrier. *Am. J. Physiol.* **238**, R421-31.

Siegal T., Rubinstein R., Bokstein F., Schwartz A., Lossos A., Shalom E., Chisin R., Gomori J. M. (2000) In vivo assessment of the window of barrier opening after osmotic blood-brain barrier disruption in humans. *J. Neurosurg.* **92**, 599-605.

Sun W. S., Misao R., Iwagaki S., Fujimoto J., Tamaya T. (2002) Coexpression of growth arrest-specific gene 6 and receptor tyrosine kinases, Axl and Sky, in human uterine endometrium and ovarian endometriosis. *Mol. Hum. Reprod.* **8**, 552-8.

Ueno E., Haruta T., Uno T., et al (2001) Potential role of Gab1 and phospholipase C-gamma in osmotic shock-induced glucose uptake in 3T3-L1 adipocytes. *Horm. Metab. Res.* **33**, 402-6.

Vajkoczy P., Knyazev P., Kunkel A., et al (2006) Dominant-negative inhibition of the Axl receptor tyrosine kinase suppresses brain tumor cell growth and invasion and prolongs survival. *Proc. Natl Acad. Sci. USA* **103**, 5799-804.

Weinger J. G., Gohari P., Yan Y., Backer J. M., Varnum B., Shafit-Zagardo B. (2008) In brain, Axl recruits Grb2 and the p85 regulatory subunit of PI3 kinase; in vitro mutagenesis defines the requisite binding sites for downstream Akt activation. *J. Neurochem.* In press.

Weksler B. B., Subileau E. A., Perriere N., et al (2005) Blood-brain barrier-specific properties of a human adult brain endothelial cell line. *FASEB. J.* **19**, 1872-4.

LEGEND TO FIGURES

Fig. 1. Tyrosine phosphorylation of Axl induced by mannitol.

(A): Detection of tyrosine phosphorylated proteins using antibody array. CECs were treated with 20% mannitol for 30 min. The antibody array was incubated with the cell homogenate and stained with anti-phosphotyrosine antibody. Identity of the proteins of interest was determined from the position on the membrane.

(B, C): Detection of phospho-Axl using immunoprecipitation. CECs were treated with 20% mannitol for 30 min. Immunoprecipitation was performed using anti-phosphotyrosine antibody and blots were stained with anti-Axl antibody (B) or the samples were immunoprecipitated using anti-Axl antibody and Western-blot was performed with anti-phosphotyrosine antibody (C). Representative blots of three independent experiments are shown. Arrows indicate the phosphorylated 140 kDa Axl protein. Arrowheads indicate cleavage products. β-actin was used as loading control.

Fig. 2. Activation of Akt in response to hyperosmotic mannitol in cerebral endothelial cells. Cells were transfected with Axl siRNA construct or Lipofectamine alone and treated with 20% mannitol for 30 min.

(A): Axl and its degradation products disappear after silencing.

(B): Activation of Axl in response to hyperosmotic mannitol induces phosphorylation of Akt. Blots were stained with anti-phospho-Akt (upper blot) or anti-Akt (lower blot) antibodies. Representative blots of two independent experiments are shown.

Fig. 3. Effect of mannitol on the cleavage of Axl. CECs were treated with 20% mannitol for 30 min and blots were stained with anti-Axl antibody. Arrows indicate the location of the whole Axl protein, arrowheads show the degradation products of Axl (A). One representative of ten independent experiments is presented.

(B): Time and concentration dependence of Axl degradation. CECs were treated with 10 or 20% mannitol for 10, 30 or 60 min and blots were stained with anti-Axl antibody.

Fig. 4. Immunofluorescence staining of Axl in CECs. CECs were cultured on glass coverslips, treated with 20% mannitol for 30 min, fixed and stained with anti-Axl antibody. One representative image of three independent experiments is shown. Scale bar = 20 μm.

Fig. 5. Expression of Axl and Gas6 mRNA in CECs. Real-time PCR was performed to assess the expression of Axl and Gas6 in response to mannitol. The housekeeping gene GAPDH was used as internal control. Data represent percentage values compared to control (mean ± SEM) calculated from four independent experiments. C = control, Ma = mannitol.

Fig. 6. Specificity of hyperosmotic stress-induced Axl degradation.

(A): Effect of different osmotic agents on the degradation of Axl. Cells were treated with 1.1 M mannitol, arabinose, urea or 0.55 M NaCl, respectively for 30 min.

(B): Effect of different stress factors on the degradation of Axl. Cells were treated with: 20% mannitol, 10 μM DMNQ or 8 g/l glucose, respectively.

(C): Degradation of Axl in MDCK and RG2 cells in response to mannitol treatment. The first two panels show the same blot with different exposure times to visualize changes in Axl and its degradation products. β-actin was used as loading control.

Fig. 7. Mechanism of Axl degradation. Cells were treated with 20% mannitol for 30 min in the presence or absence of different inhibitors: NFκB inhibitor (10 μM PDTC), Rho-kinase inhibitor (10 μM Y27632), L-type calcium channel blocker (10 μM verapamil) (A), calpain inhibitor (10 μM calpeptin), PKC inhibitor (1 μM bisindolylmaleimide), caspase inhibitor (25 μM zVAD), proteasome inhibitor (50 μM MG132), PI3kinase inhibitor (1 μM wortmannin), ERK 1/2 inhibitor (10 μM U0126) and Src inhibitor (10 μM PP1) (B) or protease inhibitors (100 μM E64, 50 μM leupeptin, 10 μM pepstatin) (C). β-actin was used as loading control.

Fig. 8. Role of metalloproteinases and of the proteasome in Axl degradation.

(A): The metalloprotease inhibitor GM6001 was able to inhibit Axl degradation. One representative of five independent experiments is shown.

(B): Densitometric analysis of Axl Western-blots. Data represent percentage values of the 140 kDa Axl band intensity compared to control (mean ± SD) calculated from five independent experiments. *: $p<0.001$ compared to control using t-test.

(C): Role of the proteasome. Protein samples were prepared from CECs treated with 20% mannitol and 50 μM MG132 either in TritonX-100 containing buffer or detergent-free buffer. One representative of three independent experiments is presented. β-actin was used as loading control.

Fig. 9. Relationship between degradation and phosphorylation of Axl.

(A): Time course of Axl phosphorylation (A, upper blot) and Axl degradation (A, lower blot). Cells were treated with 20% mannitol for the indicated times. Immunoprecipitation was

performed using anti-phosphotyrosine antibodies. Axl Western-blot was performed from the immunoprecipitated samples (A, upper blot) and the cell lysates (A, lower blot).

(B): Phosphorylation of the degradation products. Cells were treated for 30 min with 20% mannitol or 50 μM pervanadate or 20% mannitol and 10 μM GM6001 or 20% mannitol and 100 μM genistein, respectively. Immunoprecipitation was performed using anti-phosphotyrosine antibody, followed by Axl Western-blot. Double arrowheads indicate the phosphorylated cleavage products of mannitol-treated samples. β-actin was used as loading control.

(C): GM6001 does not influence phosphorylation of Akt. Cells were treated with 20% mannitol for 30 min in the presence or absence of 10 μM GM6001 and blots were stained with anti-phospho-Akt (upper blot) or Akt (lower blot) antibodies.

(D): Investigation of Axl using two-dimensional electrophoresis combined with Western-blot. Cells were treated for 30 min with 20% mannitol. Proteins of cell lysates were separated in two dimensions based on their isoelectric point and molecular weight, followed by Western-blot analysis using anti-Axl antibody.

Fig. 10. Role of Axl in mannitol-induced apoptosis.

(A): Silencing of Axl.

(B): Investigation of apoptosis after Axl silencing and mannitol treatment. Cells were cultured on glass coverslips and were transfected with Axl siRNA, scrambled RNA construct or treated with Lipofectamine alone, followed by treatment with 20% mannitol for 3 h. The rate of apoptosis was determined based on cleaved caspase-3 immunostaining. Values represent the mean ± SD calculated from two independent experiments. $p<0.05$ among all groups except Lipofectamine and scrambled, using ANOVA and LSD post hoc test.

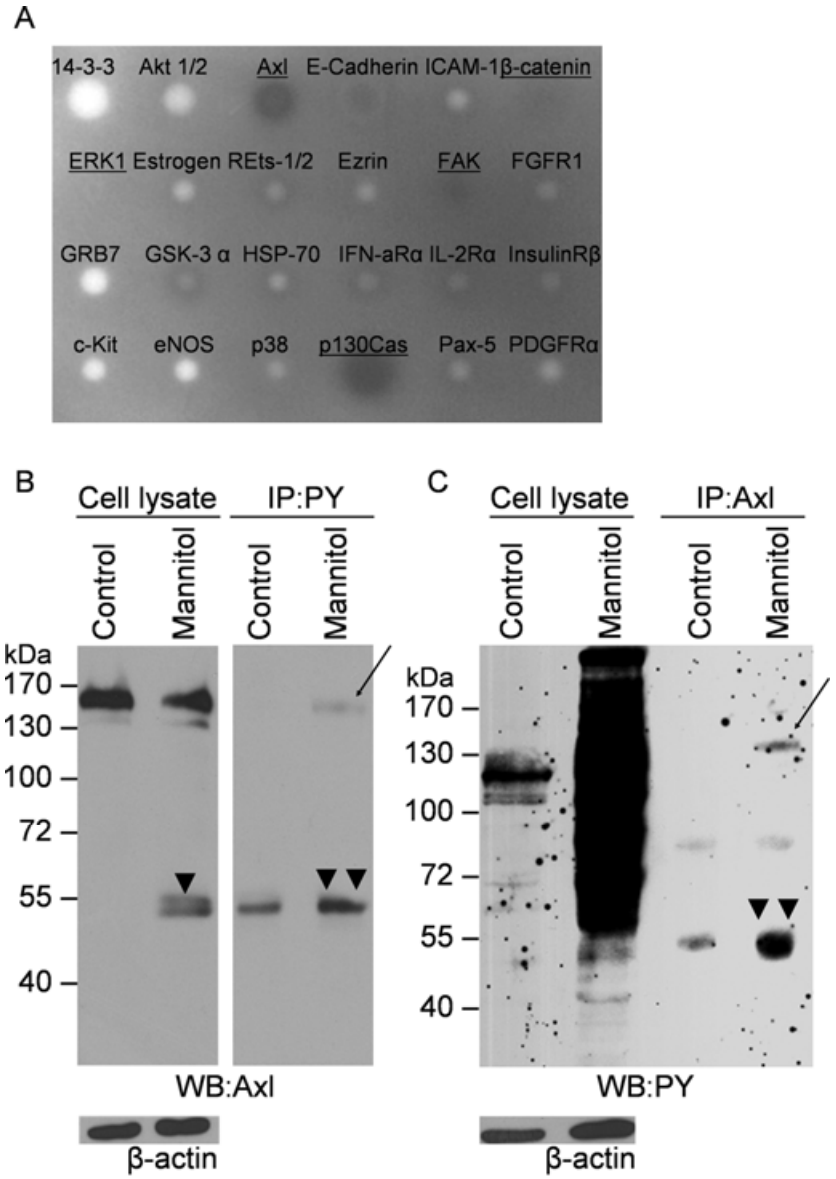
A
14-3-3
Akt 1/2
Axl
E-Cadherin
ICAM-1
β-catenin
ERK1
Estrogen REts-1/2
Ezrin
FAK
FGFR1
GRB7
GSK-3 α
HSP-70
IFN-aRα
IL-2Rα
InsulinRβ
c-Kit
eNOS
p38
p130Cas
Pax-5
PDGFRα
B
Cell lysate
IP:PY
Control
Mannitol
Control
Mannitol
kDa
170
130
100
72
55
40
WB:Axl
β-actin
C
Cell lysate
IP:Axl
Control
Mannitol
Control
Mannitol
kDa
170
130
100
72
55
40
WB:PY
β-actin

Fig. 1.

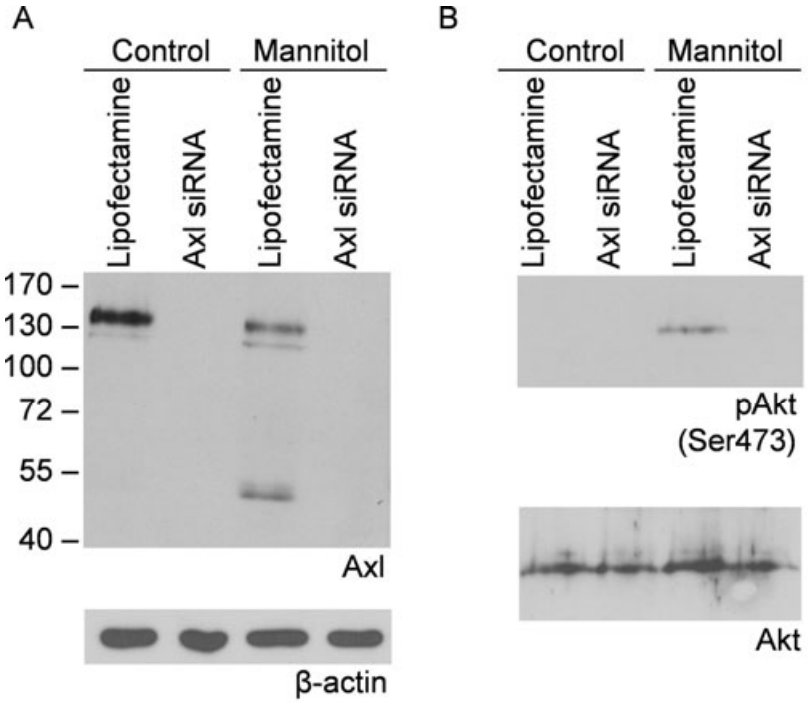
A
Control
Mannitol
Lipofectamine
Axl siRNA
Lipofectamine
Axl siRNA
170 –
130 –
100 –
72 –
55 –
40 –
Axl
β-actin
B
Control
Mannitol
Lipofectamine
Axl siRNA
Lipofectamine
Axl siRNA
pAkt
(Ser473)
Akt

Fig. 2.

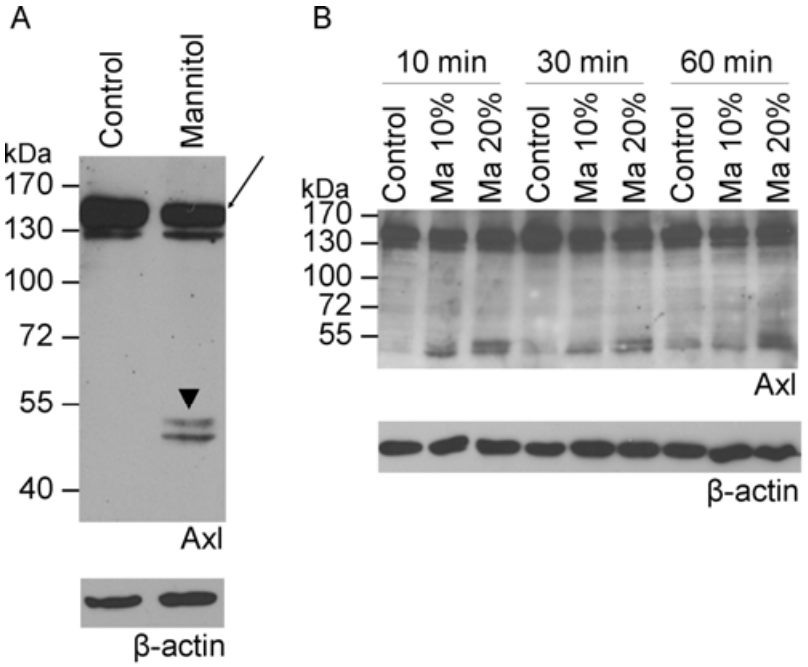
A
Control
Mannitol
kDa
170
130
100
72
55
40
Axl
β-actin
B
10 min
30 min
60 min
Control
Ma 10%
Ma 20%
Control
Ma 10%
Ma 20%
Control
Ma 10%
Ma 20%
kDa
170
130
100
72
55
Axl
β-actin

Fig. 3.

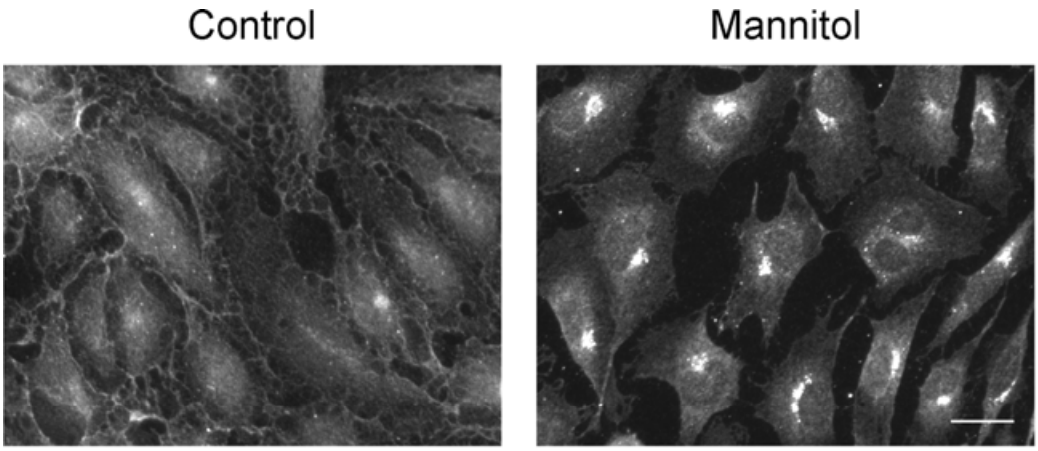

Fig. 4.

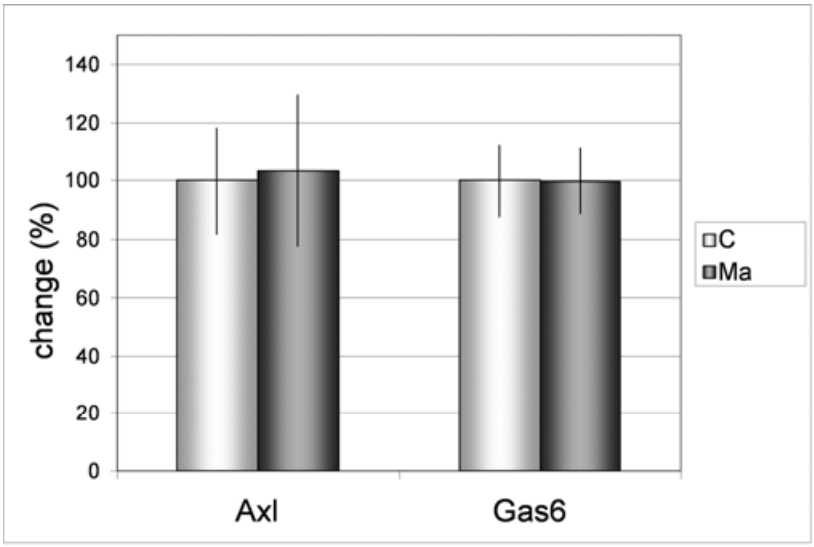

Fig. 5.

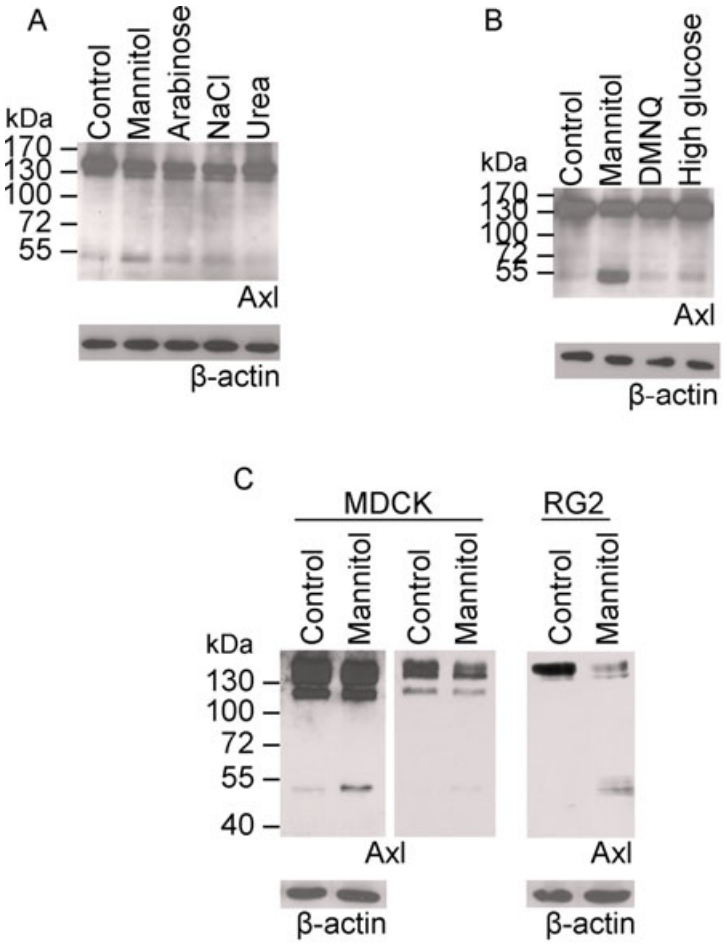
A
Control
Mannitol
Arabinose
NaCl
Urea
kDa
170
130
100
72
55
Axl
β-actin
B
Control
Mannitol
DMNQ
High glucose
kDa
170
130
100
72
55
Axl
β-actin
C
MDCK
RG2
Control
Mannitol
Control
Mannitol
Control
Mannitol
kDa
130
100
72
55
40
Axl
Axl
β-actin
β-actin

Fig. 6.

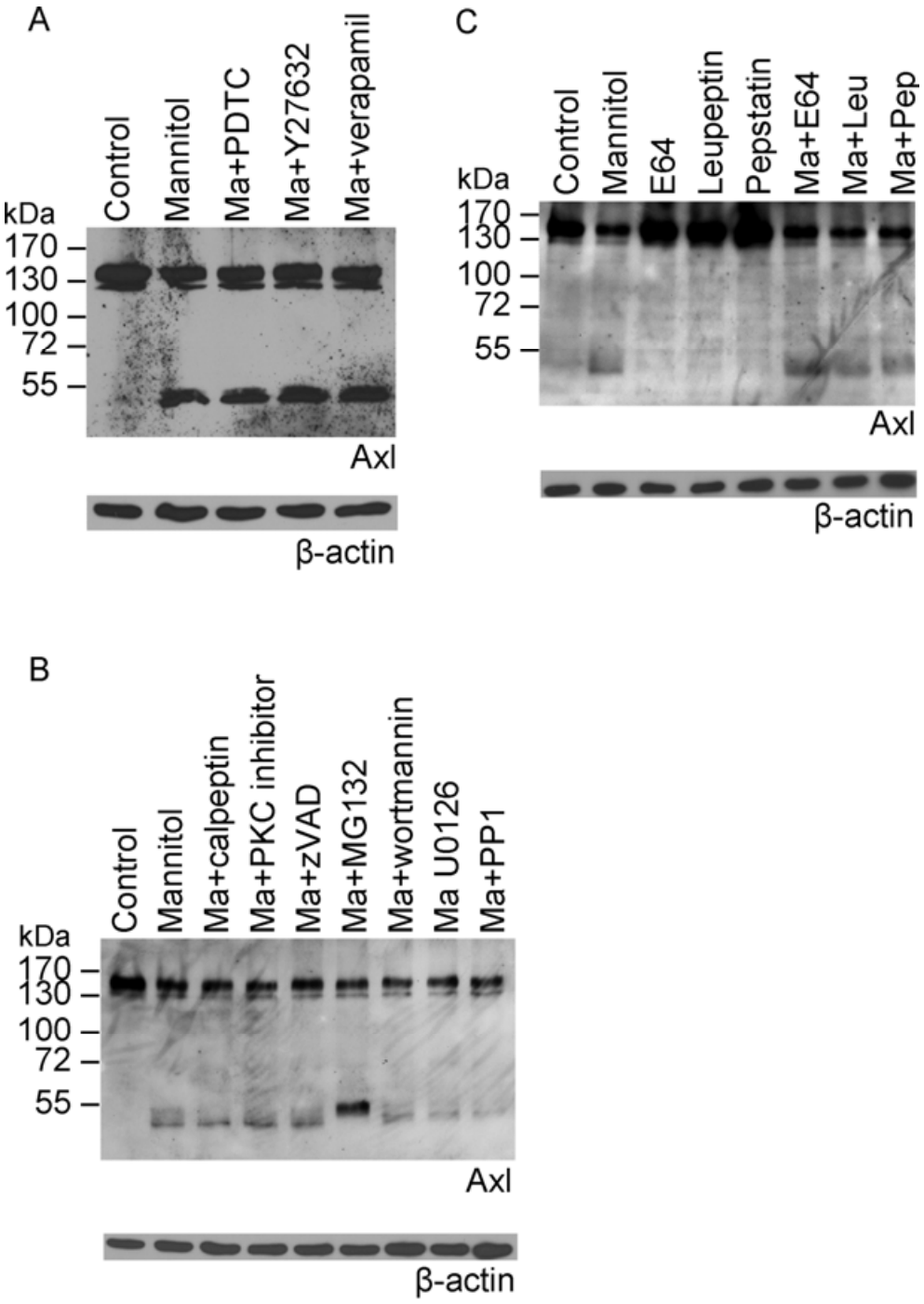
A
Control
Mannitol
Ma+PDTC
Ma+Y27632
Ma+verapamil
kDa
170
130
100
72
55
Axl
β-actin
C
Control
Mannitol
E64
Leupeptin
Pepstatin
Ma+E64
Ma+Leu
Ma+Pep
kDa
170
130
100
72
55
Axl
β-actin
B
Control
Mannitol
Ma+calpeptin
Ma+PKC inhibitor
Ma+zVAD
Ma+MG132
Ma+wortmannin
Ma U0126
Ma+PP1
kDa
170
130
100
72
55
Axl
β-actin

Fig. 7.

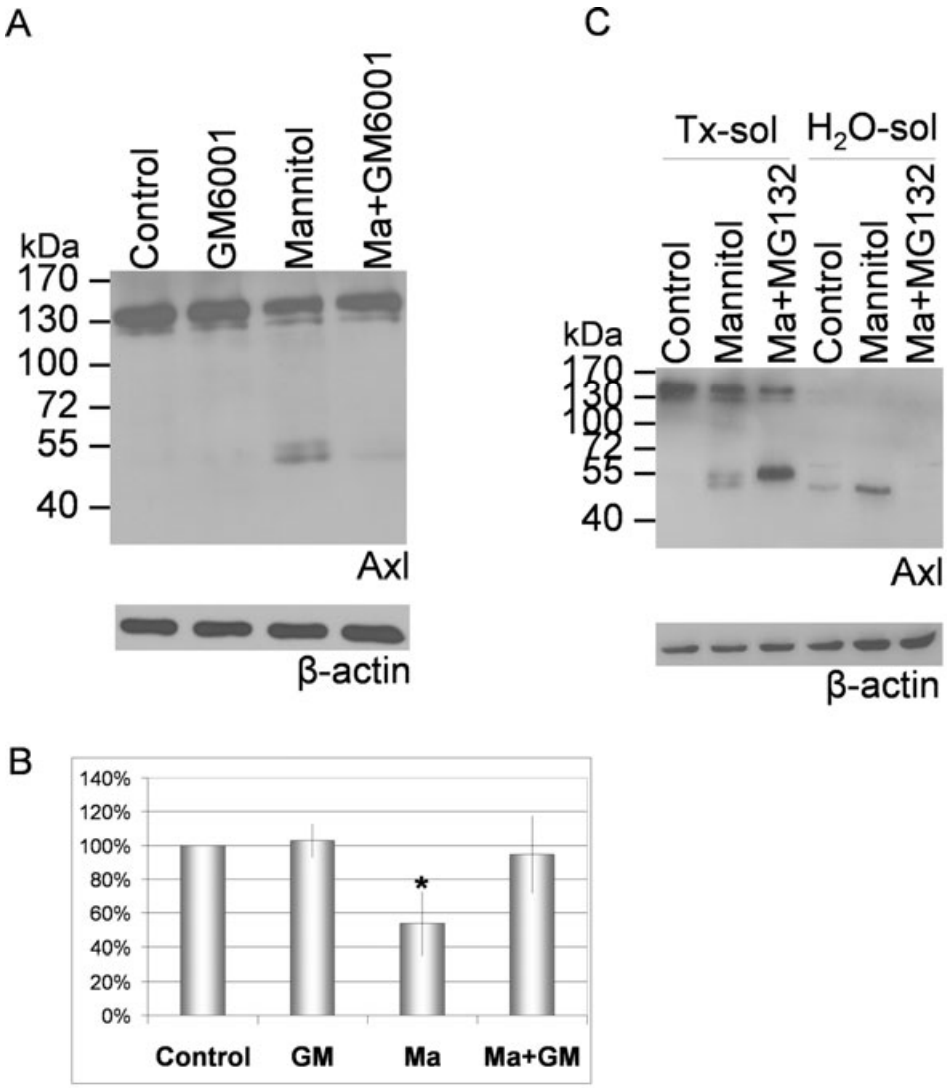
A
Control
GM6001
Mannitol
Ma+GM6001
kDa
170
130
100
72
55
40
Axl
β-actin
C
Tx-sol
H2O-sol
Control
Mannitol
Ma+MG132
Control
Mannitol
Ma+MG132
kDa
170
130
100
72
55
40
Axl
β-actin
B
140%
120%
100%
80%
60%
40%
20%
0%
*
Control
GM
Ma
Ma+GM

Fig. 8.

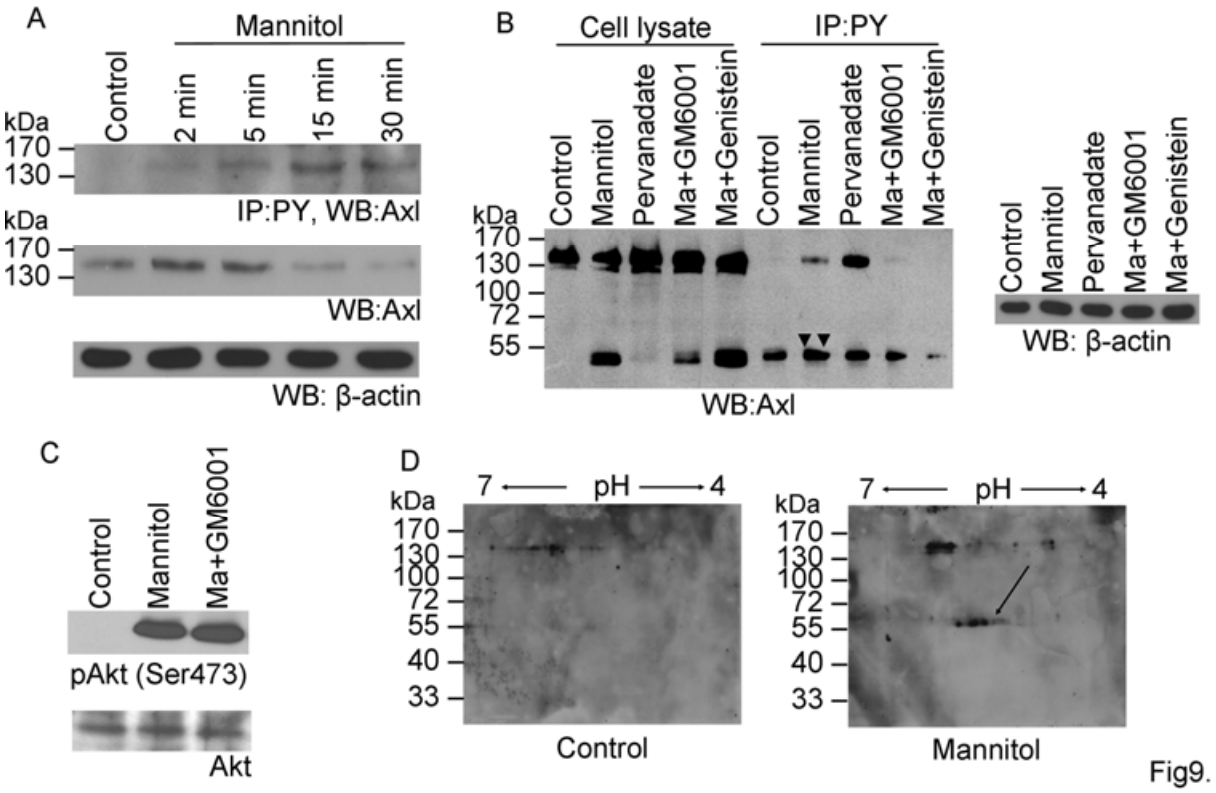
A
Mannitol
Control
2 min
5 min
15 min
30 min
kDa
170
130
IP:PY, WB:Axl
WB:Axl
WB: β-actin
B
Cell lysate
IP:PY
Control
Mannitol
Pervanadate
Ma+GM6001
Ma+Genistein
kDa
170
130
100
72
55
WB:Axl
WB: β-actin
C
pAkt (Ser473)
Akt
D
7
pH
4
kDa
170
130
100
72
55
40
33
Control
Mannitol

Fig9.

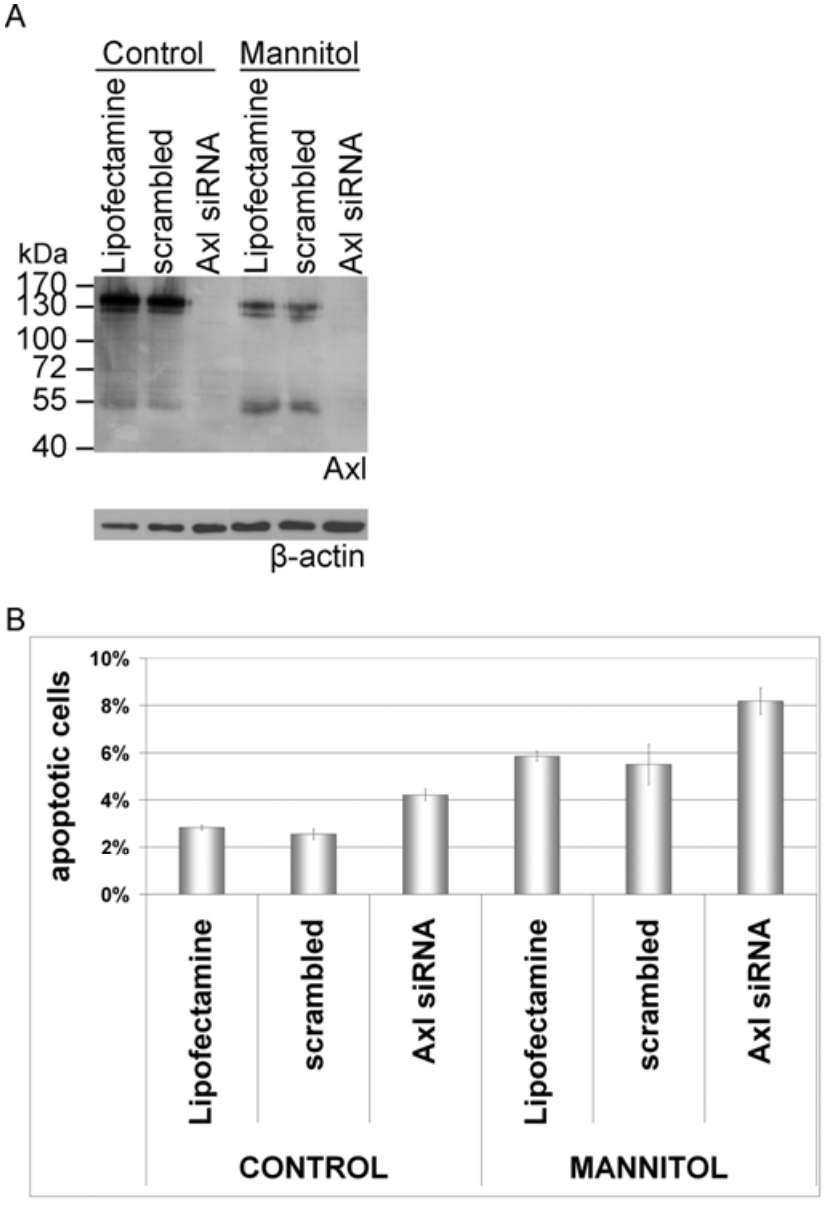
A
Control
Mannitol
Lipofectamine
scrambled
Axl siRNA
Lipofectamine
scrambled
Axl siRNA
kDa
170
130
100
72
55
40
Axl
β-actin
B
apoptotic cells
10%
8%
6%
4%
2%
0%
Lipofectamine
scrambled
Axl siRNA
Lipofectamine
scrambled
Axl siRNA
CONTROL
MANNITOL

Fig. 10.